

Anodized Aluminum Oxide Membranes as Templates for Nanoscale Structures

*Catherine Y. Han, Z.L. Xiao, H.H. Wang, G.A. Willing, U. Geiser,
U. Welp, W.K. Kwok, S.D. Bader, and G.W. Crabtree*

Materials Science Division, Argonne National Laboratory, Argonne, IL 60439, USA

Porous anodic aluminum oxide (AAO) membranes have attracted significant interest during recent years because of the fact that AAO can be made conveniently and inexpensively, yet they are extremely useful in nanoscience studies. Pore diameter (5-300 nm), and pore-pore distance (25-500 nm) can be easily controlled by varying the anodizing conditions. Highly ordered, straight nanopores in hexagonally close-packed arrays with domain sizes of approximately $2.5 \times 2.5 \mu\text{m}^2$ and aspect ratios as high as 1000 can be achieved. The nanopores within the AAO membranes are used as templates for fabricating various nanoscale structures, such as the first successful fabrication of superconducting lead nanowires with diameters of 60 and 200 nm. Lead was electrodeposited into the nanopores of AAO, and bismuth quantum nanotubes were fabricated, utilizing a newly developed high-temperature sintering method. It is also possible to construct highly ordered anti-dot arrays by coating the surfaces of the porous AAO membranes with magnetic materials. Significant enhancement of the critical field in superconducting Pb nanowires and an abnormal magnetoresistance in Ni magnetic anti-dot arrays are found in these samples. The preparation, characterization of AAO and its application in fabricating various nanowires, nanotubes, and nanoscale antidots will be presented. Work at ANL is supported by the U.S. DOE/BES Materials Science under contract W-31-109-ENG-38.

For more information, contact:

Dr. Catherine Y. Han
9700 South Cass Avenue,
Argonne National Laboratory,
Argonne, IL60439
Phone-630-252-1499
Fax-630-252-9151
E-mail: cyhan@anl.gov

Introduction

The fabrication of functional, nanostructured arrays in a well-controlled way is one of the exciting frontiers in today's science and technology. In recent years, numerous methods have been utilized, with varying degree of success, to fabricate nanostructures with smaller size, higher regularity and reliability because of the potential applications in electronic, optical, and magnetic nanodevices. Compared to conventional lithographic techniques such as UV, x-ray, electron beam or scanning probe lithography, template method based on self-organized nanoporous arrays present an inexpensive, high throughput, and efficient process for achieving nanosize periodic structures with high aspect ratio over a large area. Anodic films on Al formed by anodization have been used commercially as keying layers for the retention of organic coatings and protection of Al substrates against corrosion and abrasion for at least 80 years¹. The anodic aluminum oxide (AAO) membranes formed in acidic solutions have a porous structure and mainly consist of amorphous Al_2O_3 . The geometry of porous anodic alumina can be schematically represented as a honeycomb structure that is characterized by a close-packed array of columnar hexagonal cells, each containing a central pore normal to the substrate (Figure 1). Only an approximately hexagonal arrangement of these pores with low periodicity had been yielded through conventional anodization in the past 70 years². However, recently, AAO films with a perfect hexagonal pore arrangement over several μm^2 , have been achieved through a two-step anodization process³⁻⁸. Films created through this technique display a high degree of hardness and wear resistance, have excellent corrosion resistance and a high pore density and are thermally stable. The pore diameter, pore-pore distance and depth of the pores can be easily controlled by choosing appropriate anodizing conditions such as temperature, type and concentration of electrolyte, anodizing voltage and duration of the anodization⁹. All these merits make AAO membranes an attractive template for the fabrication of ordered arrays of nanowires⁷, nanodots, anti-dots, and nanotubes. The pores can serve as a host to other material classes, such as magnetic or thermoelectronic materials. The integration of porous oxides with these other classes of materials allows for the rapid and inexpensive fabrication of complex composite materials.

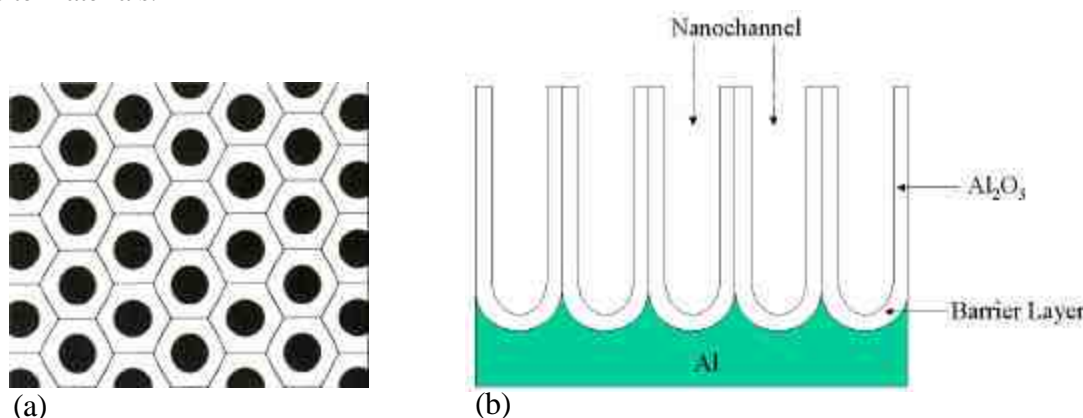


Figure 1. The geometry of porous anodic alumina can be schematically represented as a honeycomb structure which is characterized by a close-packed array of columnar hexagonal cells, each containing a central pore normal to the substrate. Top view of AAO membrane (a). Side view of the typical alumina structure fabricated using bulk aluminum (b).

Experimental Section

High purity aluminum foil (99.998%) with thickness of 250-500 μm was first degreased in acetone for 10 min and dried at 100 $^{\circ}\text{C}$, annealed at 500 $^{\circ}\text{C}$ under an Ar atmosphere for 4 hr to enhance the grain size, and electropolished in a solution of HClO_4 (60 wt%) and EtOH (1:8 in volume) at a current density of 100 mA/cm^2 and a temperature of 0 $^{\circ}\text{C}$ for 10 min to generate a smooth surface. The anodization was carried out under constant anodizing voltage, in 0.3 M aqueous solutions of either oxalic or sulfuric acid at 3.0 $^{\circ}\text{C}$ for 24 hr (Figure 2). The resulting 70 μm thick, porous alumina layer was stripped away from the Al substrate by etching the sample in a solution contains 6 wt% phosphoric acid and 1.8 wt% chromic acid at 60 $^{\circ}\text{C}$ for 12 hr. After removal of the initial AAO film, the anodization was repeated under the same conditions for hours needed to reach desired film thickness. A freestanding AAO membrane with a highly ordered array of nanopores can then be obtained by selectively etching away the unreacted Al in a saturated HgCl_2 solution or a mixture of 0.1M CuCl_2 and HCl (37 wt%) in 4:1 (v/v). The pore array was studied by field emission scanning electron microscopy (SEM) (Hitachi S-4700-II), atomic force microscopy (AFM) (DI dimension 3000 with Nanoscope IIIA controller), and small angle X-ray scattering (SAXS) (Advanced Photon Source at Argonne National Laboratory).

A dome-shaped aluminum oxide layer, with a thickness of 10-30 nm, depending on the anodizing voltage, forms at the bottom of each single nanopore during anodization (Figure 1b). To remove this barrier layer, a protective polymer layer was first coated on the top surface of the AAO membrane to prevent etching of the surface structure and uneven diffusion of acid into the nanopores. The membrane was then immersed in 200 ml 5.0 wt% phosphoric acid at 30.0 $^{\circ}\text{C}$ for varying periods of time, rinsed with distilled water and dried under ambient conditions. The barrier layer removal and pore widening process was then studied by AFM and SEM.

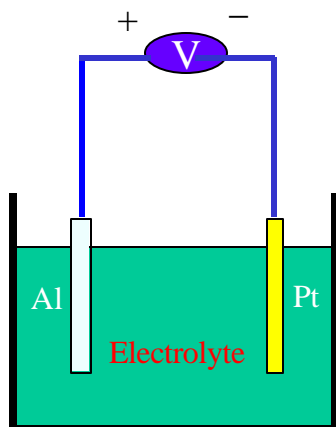


Figure 2. Anodization can be done inexpensively and conveniently in a simple lab setup.

Results and discussion

Although the electropolishing process yields a surface with a roughness of less than 10 nm over a 5 μm area, there are still small pits and bumps with density as high as 10^{12} cm^{-2} , which could act as

nucleation centers for pore growth². The pore density is very high and the pore initiation sites spread randomly over the Al surface at the beginning of anodization. Ordering of the cell arrangement increases with the anodizing time after the steady state growth of the porous structure is established³. Therefore, at least two steps of anodization are needed for a membrane with highly ordered pore arrays. Long time first-step anodization and stripping of the resulting AAO film from the Al substrate not only removes the disordered AAO membrane but also leaves a highly ordered dimple array on the aluminum surface. Each dimple will initialize a new pore during the second anodization step, which is carried out under the same conditions as the first³.

We have carried out two-step anodizations at 10, 15, 20, and 25 V in 0.3 M sulfuric acid, and 10, 30, 40, 50, 60, and 80V in 0.3 M oxalic acid at 3 °C. In the past, SEM and AFM had been used exclusively as characterization tools for AAO membranes¹⁰. While these techniques are ideal for local characterization of the structure and morphology of an AAO film, their bulk characterization abilities are limited. Because of the insulator behavior of alumina, its characterization by SEM can be very difficult, and only information of the surface structure can be obtained. AFM has a very limited penetration into the pores and thus is not suitable to characterize the pore structure of thick films. SAXS has been used for the first time in our lab to characterize the cell configuration of films with thicknesses up to 100 μm. The advantage of using SAXS is that, as a bulk characterization technique, it can be used to determine the average morphology over large areas and through the whole depth of the nanochannel as the X-ray beam is 200×400 μm² in area (covering ~200 domains) and penetrates the film completely.

Two pieces of information can be obtained from SAXS data: pore-pore distance and the degree of pore ordering (Figure 3a,b). SAXS data show that self-ordering takes place at 25 V in sulfuric acid, 40 and 50 V in oxalic acid solution, corresponding to pore-pore distance of 63 nm, 100 nm, and 125 nm respectively. Longer first-step anodization times increase the size of ordered domains in AAO only under these specific anodization voltages and little or no ordering was observed without the appropriate voltage conditions. The ordered structure at 50 V anodization has never been reported before. This has been verified through SEM (Figure 3c) and AFM imaging.

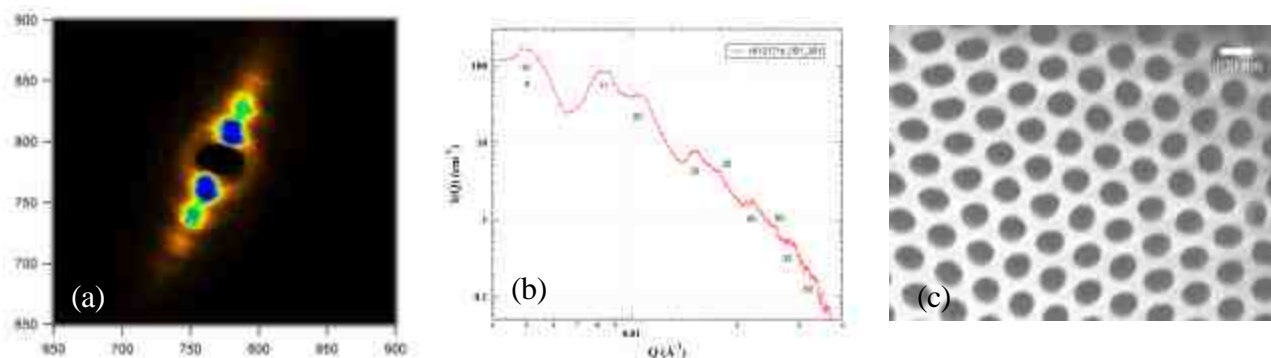


Figure 3. (a) A 2D false color image of small angle x-ray scattering intensities of a highly ordered AAO thin film. Due to a minute mismatch between the membrane and the incident beam direction, the scattering intensity is concentrated along a line corresponding to intersection of the membrane and the plane perpendicular to the beam. (b) A plot of averaged 1D spectrum showing scattering intensity as a function of scattering vector. The scattering peaks have been assigned based on a 2D hexagonally close packed model. The unit cell can be extracted from the slope of a q^2 vs. (h^2+k^2+hk) plot. For this sample, hole-to-hole distance is 116.8 nm. (c) SEM of AAO membrane anodized at 50 V showing a degree of ordering comparable to sample anodized at 40 V.

SAXS data also show that the pore-pore distance increases linearly with anodizing voltage no matter what type of electrolyte is used. The cell size increases 2.2 nm for every volt (Figure 4). SEM data shows that the pore diameter at the channel opening is independent of anodizing voltage, which is 10 nm in 0.3 M sulfuric acid and 35 nm in 0.3 M oxalic acid. It is mainly decided by the PH value of the electrolyte that determines the dissolution rate of alumina.

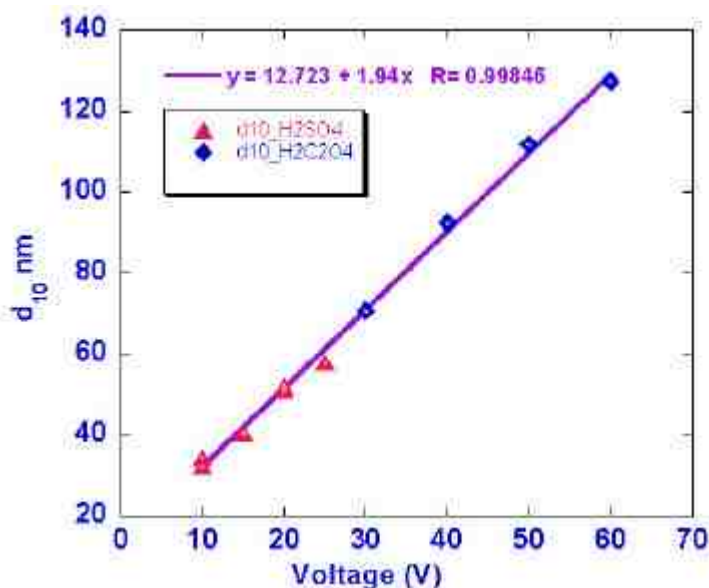


Figure 4. AAO characterization with SAXS. The crystallographic {1,0} d-spacing ($\sqrt{3}/2$ times the pore-pore distance in the hexagonal model) increases linearly with anodizing voltage, irregardless of electrolyte.

Perhaps unsurprisingly, the AAO films grow simultaneously on all Al surfaces exposed to electrolytes unless covered with an insulating polymer layer. Both the electrolyte and the Al are highly conducting while the Al_2O_3 is highly insulating. Thus, the potential throughout either the solution or the metal is essentially constant, and the gradient is normal to the surface and its magnitude independent of location (only depends on oxide thickness and porosity). This means that complicated 3D porous AAO structures can be formed by anodizing Al with any predefined shape. In the case of anodizing a thin Al foil, AAO films formed on both sides, and they can be separated by selectively etching away the Al substrate sandwiched between them in saturated HgCl_2 aqueous solution. The cell regularity is almost identical for the two films, with the backside of the AAO films containing fewer defects than the top side (Figure 5).

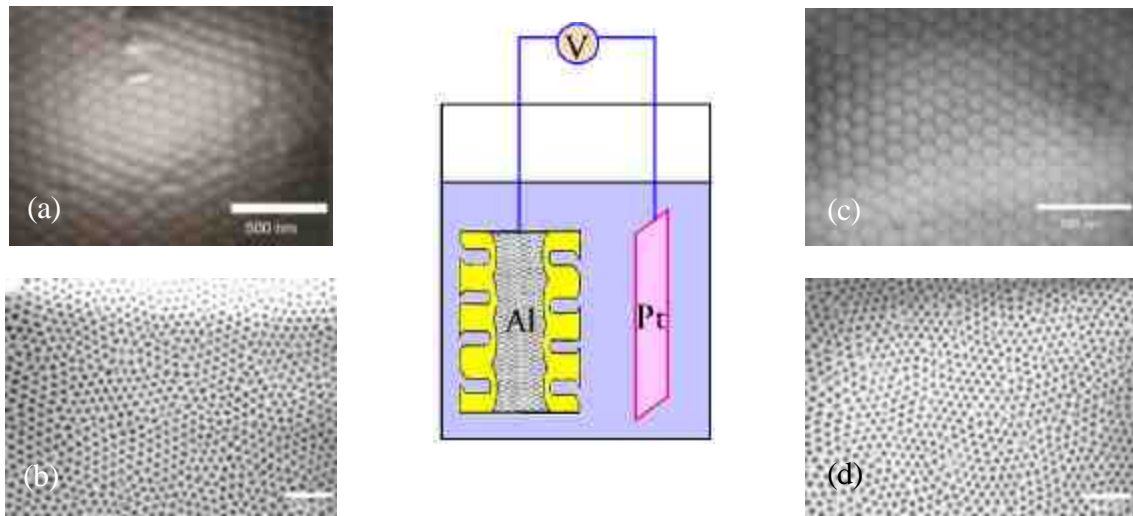


Figure 5. Two identical AAO films grow simultaneously on both sides of Al substrate. Rear layer backside (a). Rear layer topside (b). Front layer backside (c). Front layer topside (d).

A semispherical shell with homogeneous thickness known as the barrier layer (Figure 1b) develops at the bottom of every single nanopore during the anodization process, which hasn't attracted much attention in the applications literature. However, removal of the barrier layer is required, when through-hole AAO membranes are needed. Examples for such applications include using AAO membranes for energy-efficient gas-separating membranes and pattern-transfer masks for e-beam evaporation³, reactive ion etching¹¹, or molecular-beam epitaxial growth¹². Three methods had been used to open the barrier oxide layer: chemical etching³, ion milling¹³, and plasma etching¹¹. Ion milling and plasma etching require expensive equipment and can only work on one small area at a time and thus are cost and time intensive. Chemical etching, on the other hand, is inexpensive, fast, convenient, reliable, and can be used to etch samples with large dimensions. Very little study has been done in the past to reveal the barrier layer opening process. Our experimental results show that if the chemical etching is done properly, holes in the barrier layer from less than 10 nm in diameter up to 90% of the cell size can be obtained (Figure 6c-f). Once there is an opening in the barrier layer, the etching solution can diffuse into the pore and expand the pore along its entire length. Figure 6g shows the rate of opening as a plot of hole diameter with respect to time. Such a plot should prove useful in controlling the size of the opening in the barrier layer under a fixed pore-pore distance. This is an interesting finding since highly ordered pore arrays with sub-10-nm diameter has not been demonstrated by self-assembly. More importantly, very interesting and unique nanostructures generated before the complete removal of the barrier layer had been observed by AFM imaging, which have potential application as templates to grow nanostructured thin films (Figure 6a-d).

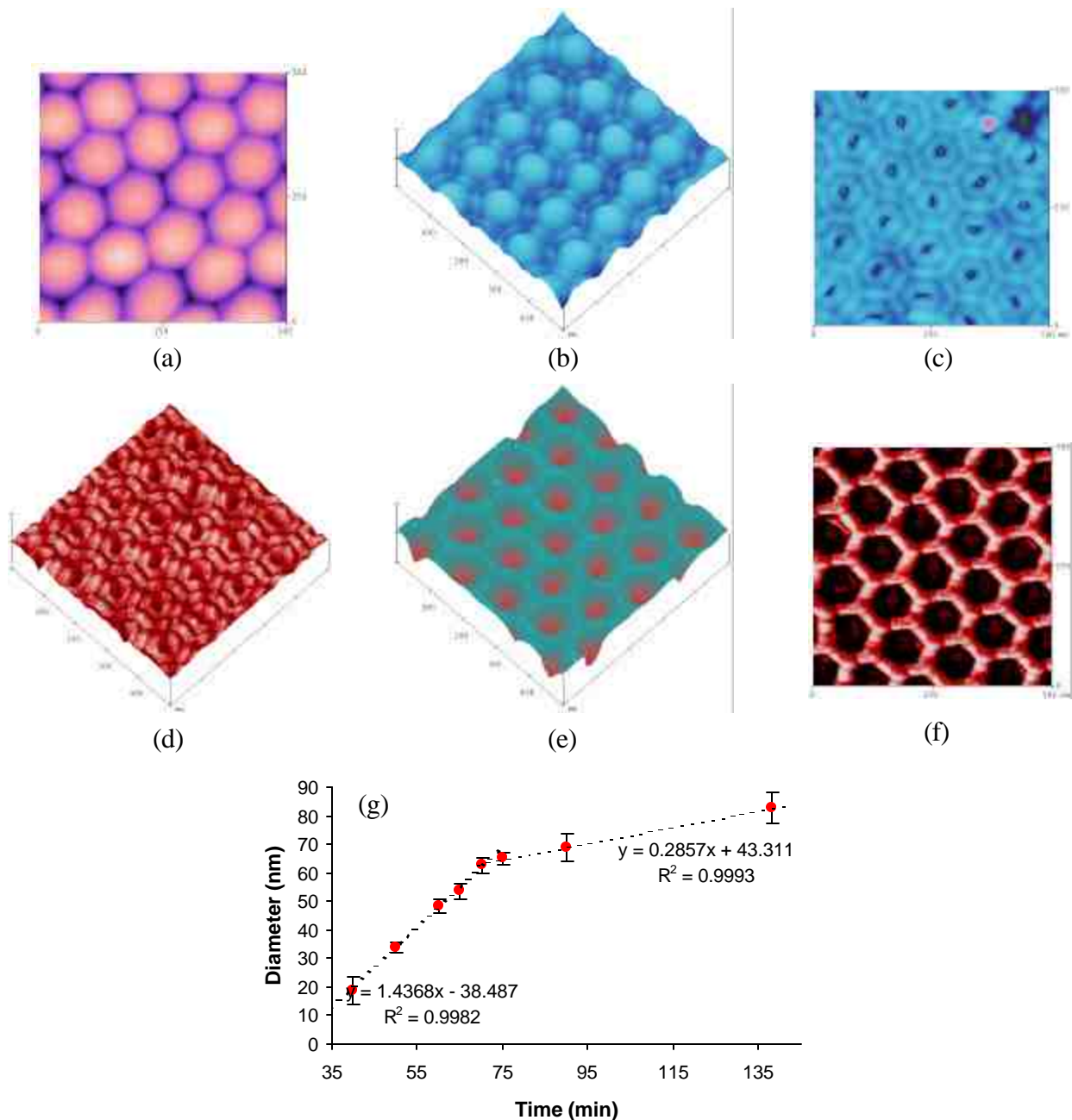


Figure 6. AFM study of the barrier layer removal process for an AAO membrane made in 0.3 M oxalic acid at 40 V, 3 °C by anodizing for 24 hr twice. (a) Freshly made barrier layer has hexagonally close packed hemispheres. (b) Barrier layer of AAO film was etched in 5 wt% phosphoric acid at 30 °C for 30 min, hemispheres become smaller and a hexagon cell appears. (c) The barrier layer was opened to 10 nm at 40 min of etching. (d) A 30 nm opening was obtained after 50 min of etching. (e) Barrier layer was completely removed and the pore was opened to 60 nm after 75 min of etching. (f) The cell wall become very thin and pore was expanded to 85 nm after 138 min of etching. (g) Plot of pore diameter versus etching time.

Nanostructures including nanowires, nanotubes, and antidots are promising subjects for research into the novel phenomena induced under confined geometries and have potential applications in nanoscale devices. One approach in fabricating these nanostructures is the so-called “template synthesis” that utilizes nanopores in porous membranes as templates. The ultra-high-density magnetic antidot array, a promising candidate for magnetic storage applications, was prepared by depositing nickel onto AAO membranes by dc magnetron sputtering at 25 °C under 10^{-4} Pa⁸. The antidot arrays made on AAO membrane with 100 nm pore-pore distance have pore density of $10^{10}/\text{cm}^2$, which corresponds to a storage density of 10 Gbits/cm² (Figure 7). FESEM showed the pore size decreases with increasing thickness of deposited nickel.

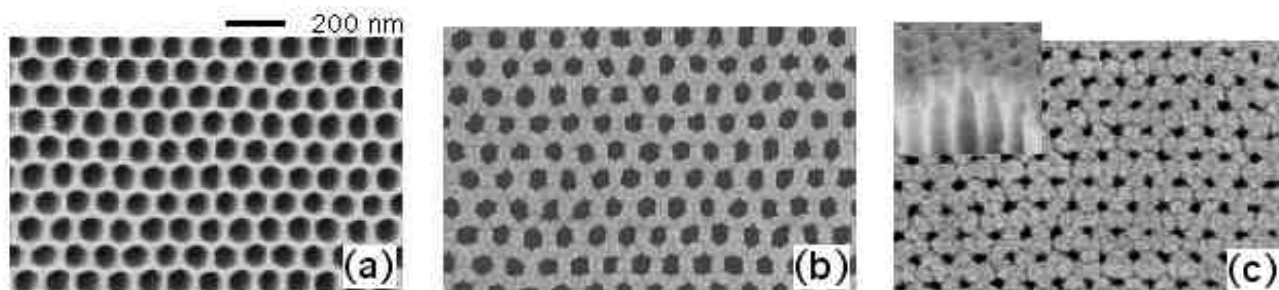


Figure 7. SEM images of the nickel antidot arrays on AAO membrane. Thickness of deposited nickel layers are 5 nm (a), 50 nm (b), and 100 nm (c). The inset in (c) is the side view of the 100 nm thick antidot array.

The magnetotransport and magnetization data measure at 280 K for the 100-nm-thick film are summarized in Figure 8. Whereas the transverse magnetoresistance shows similar overall behavior and magnitude as seen in the continuous film (Figure 8a), unusual nonmonotonic behavior is observed in the longitudinal magnetoresistance (Figure 8b), which we attributed to the inhomogeneous rotation of magnetic moments with respect to the applied field and current directions. The magnetization curve of the antidot array exhibits a loop with enhanced values of coercive field and remnant magnetic moment, whereas the continuous film made by depositing nickel onto a glass slide has an almost reversible magnetization. We attribute this to the interplay of shape anisotropy and inhomogeneous magnetization caused by the nanoscale patterning of the magnetic film (Figure 8c).

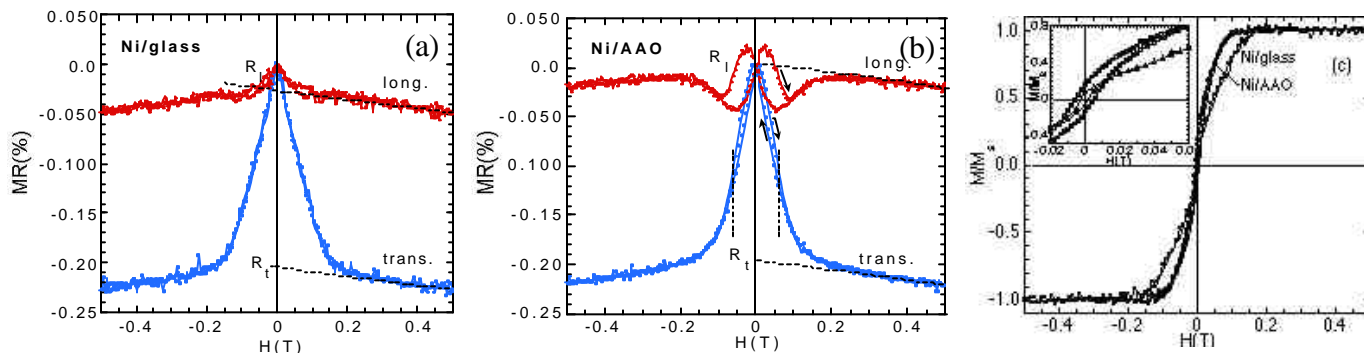


Figure 8. Magnetotransport of 100-nm-thick nickel on glass (a) and on AAO membrane (b). Comparison of the magnetization of both samples (c). The inset in (c) shows the low field magnetization on expanded scales.

problem was solved by utilizing ac electrodeposition. Better quality nanowires with higher filling percentages and narrower length distributions were made with ac electroplating. These nanowires exhibited a variety of novel properties, including localization, magnetic anisotropy, enhanced coercivity, and giant magnetoresistance. The magnetization hysteresis of 2-3 μm long Ni nanowires with a 200 nm diameter imbedded in AAO is shown in figure 9d. The easy axis is perpendicular to the nanowires. On the other hand, in 30 μm long Ni nanowires with a 60 nm diameter imbedded in AAO (Figure 9e), the easy axis intends to be parallel to the nanowires due to geometric anisotropy of this high aspect ratio structure. Such nanostructures have significant potential applications as high-density perpendicular recording media and field sensing devices, as well as being useful in fundamental scientific studies of nanomagnetism.

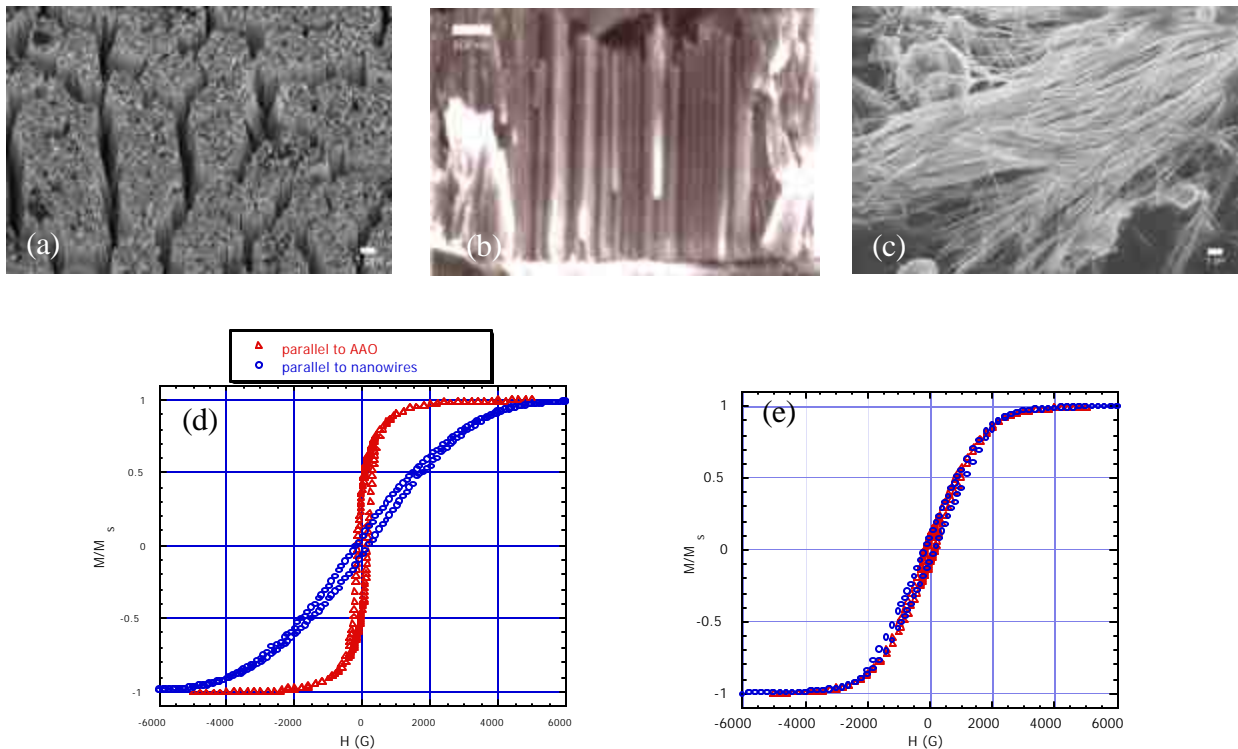


Figure 9. (a) SEM top view of Ni nanowires (200 nm diameter, 0.05 M NiCl_2 in DMSO) with AAO templates partially removed. (b) SEM cross-section view of Ni nanowires (60 nm diameter, 0.1 M NiSO_4 in H_2O) imbedded in AAO. (c) SEM of Ni nanowires (60 nm diameter, 0.05 M NiCl_2 in DMSO) with AAO template completely removed. (d) Magnetization hysteresis of 2-3 μm long Ni nanowires with 200 nm diameter imbedded in AAO. The easy axis is perpendicular to the nanowires. (e) Magnetization hysteresis of 30 μm long Ni nanowires with 60 nm diameter imbedded in AAO. The easy axis is parallel to the nanowires.

Superconducting lead nanowires were made by electrodepositing Pb into the nanopores from a 0.07 M $\text{Pb}(\text{NO}_3)_2$ aqueous solution. The experimental set up is the same as shown in figure 2. The SEM image, obtained after dissolving the AAO membrane with a 1 M NaOH aqueous solution, shows the uniform length and diameter of the Pb nanowires (Figure 10a). Transport measurements show an enhancement of the critical field (Figure 10b).

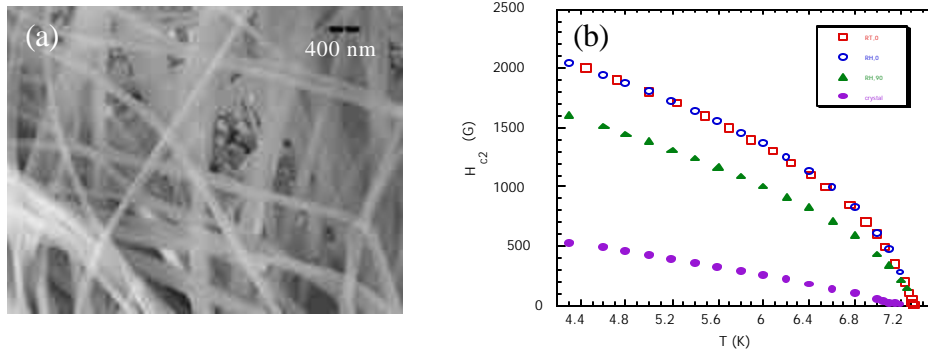


Figure 10. (a) Superconducting lead (Pb) nanowires electrodeposited into the nanopores. The SEM image was obtained after dissolving the AAO membrane with NaOH aqueous solution. (b) Transport measurements show an enhancement of the critical field.

Polymer nanotubes were made by first wetting the AAO membrane in a 1 wt% polyethylene solution in acetone, and then dried at 100 °C for 1 hr (Figure 11a). SEM images were then recorded after dissolving the AAO templates with a 1 M NaOH aqueous solution. The outer diameter of the polymer nanotubes is controlled by the AAO pore diameter and the length of the nanotubes is determined by the thickness of the AAO membrane. These nanotubes can be used as a protective insulating layer for metal nanowires.

Bi nanotubes were made by a high temperature sintering method. A bismuth layer was first electrodeposited on AAO by using a thin layer of Au as electrode. After sintering the sample at 450-650 °C, Bi nanotubes with a wall thickness of 10 nm were observed (Figure 11b).

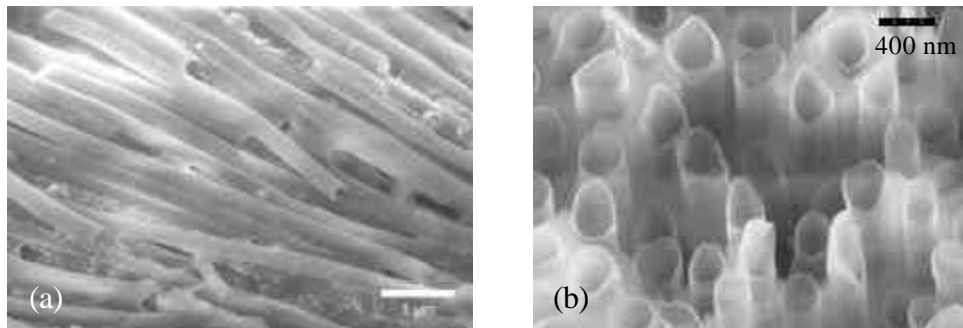


Figure 11. (a) Polyethylene nanotubes after dissolving AAO template. (b) Bi nanotubes made by a high temperature sintering method.

Conclusion

We have established several electro-chemical anodization procedures for synthesizing a new generation of anodic aluminum oxide (AAO) membranes containing large-area periodic arrays of uniform pores. The process converts aluminum foil, with thickness between 0.25 mm and 1 mm, into aluminum oxide by anodizing the foil in an acid solution. The self-organized pore diameters and pore-pore distances can be adjusted by changing the anodization voltage and the acid concentration. We have succeeded in synthesizing porous AAO membranes with pore diameters ranging from 10 nm to 200 nm by anodizing aluminum in oxalic and sulfuric acids under various reaction conditions. By utilizing the nanopores of AAO membranes as templates, we synthesized magnetic (Ni) and superconducting (Pb) nanowires with diameters down to 10 nm by electrodeposition. Polyethylene nanotubes and bismuth quantum nanotubes were synthesized with AAO membranes using a high temperature sintering method. Highly ordered antidot (hole) arrays of magnetic nickel prepared by coating the surfaces of the porous membrane show an abnormal magnetoresistance, attesting to the exciting physics of these novel nanostructures created utilizing the AAO templates.

Acknowledgments

Work at Argonne National Laboratory including access to the Advanced Photon Source and the Electron Microscopy Center is sponsored by the U. S. Department of Energy, Office of Basic Science, Division of Materials Science, under Contract W-31-109-ENG-38.

References

1. G.D. Bengough, J.M Stuart, Brit. Patent 223,994 (1923).
2. F.Li, L. Zhang, and R.M. Metzger, *Chem. Mater.*, **10**, 2470 (1998).
3. H. Masuda and M. Satoh, *Jpn. J. Appl. Phys.*, **35**, L126 (1996).
4. H. Masuda, F. Hasegawa, S. Ono, *J. Electrochem. Soc.*, **144**, L127 (1997).
5. H. Masuda, K. Yada, and A. Osaka, *Jpn. J. Appl. Phys.*, **37**, L1340 (1998).
6. H. Asoh, K. Nishio, M. Nakao, A. Yokoo, T. Tamamura, H. Masuda, *J. Vac. Sci. Technol. B.*, **19**, 569 (2001).
7. A.J. Yin, J.L. Jian, A.J. Bennett, J.M. Xu, *Appl. Phys. Lett.*, **79**, 1039 (2001).
8. Z. Xiao, C.Y. Han, U. Welp, H.H. Hau, et al., *Appl. Phys. Lett.*, **81**, 2869 (2002).
9. G.E. Thompson, *Thin Solid Films*, **297**, 192 (1997).
10. Y. Sui, J.M. Saniger, *Materials Letters*, **48**, 127 (2001).
11. J. Liang, H. Chik, A. Yin, J. Xu, *J. Appl. Phys.*, **91**, 2544 (2002)
12. X. Mei, D. Kim, H.E. Ruda, Q.X. Guo, *Appl. Phys. Lett.*, **81**, 361 (2002)
13. T. Xu, G. Zangari, and R.M. Metzger, *Nano Lett.*, **2**, 37 (2002).